First results from MFOSC-P: low-resolution optical spectroscopy of a sample of M dwarfs within 100 parsecs

A. S. Rajpurohit, Vipin Kumar, Mudit K. Srivastava, F. Allard, D. Homeier, Vaibhav Dixit, Ankita Patel

Monthly Notices
of the
ROYAL ASTRONOMICAL SOCIETY

MNRAS **492,** 5844–5852 (2020) doi:10.1093/mnras/staa163

First results from MFOSC-P: low-resolution optical spectroscopy of a sample of M dwarfs within 100 parsecs

A. S. Rajpurohit,[1]★ Vipin Kumar,[1,2]★ Mudit K. Srivastava,[1]★ F. Allard,[3] D. Homeier,[4] Vaibhav Dixit[1] and Ankita Patel[1]

[1]*Astronomy & Astrophysics Division, Physical Research Laboratory, Ahmedabad 380009, India*
[2]*Indian Institute of Techonology, 382355 Gandhinagar, India*
[3]*Univ Lyon, Ens de Lyon, Univ Lyon1, CNRS, Centre de Recherche Astrophysique de Lyon (CRAL), Ecole Normale Superieure de Lyon, F-69364 Lyon, France*
[4]*Zentrum für Astronomie der Universität Heidelberg, Landessternwarte, Königstuhl 12, 69117 Heidelberg, Germany*

Accepted 2020 January 14. Received 2020 January 12; in original form 2019 November 20

ABSTRACT

Mt Abu Faint Object Spectrograph and Camera (MFOSC-P) is an in-house-developed instrument for the Physical Research Laboratory (PRL) 1.2 m telescope at Mt Abu, India, commissioned in 2019 February. Here we present the first science results derived from the low-resolution spectroscopy programme of a sample of M dwarfs carried out during the commissioning run of MFOSC-P between 2019 February and June. M dwarfs carry great significance for exoplanet searches in the habitable zone and are among the promising candidates for the observatory's several ongoing observational campaigns. Determination of their accurate atmospheric properties and fundamental parameters is essential to constrain both their atmospheric and evolutionary models. In this study, we provide a low-resolution ($R \sim 500$) spectroscopic catalogue of 80 bright M dwarfs ($J < 10$) and classify them using their optical spectra. We have also performed spectral synthesis and χ^2 minimization techniques to determine their fundamental parameters regarding effective temperature and surface gravity by comparing the observed spectra with the most recent BT-Settl synthetic spectra. The spectral type of M dwarfs in our sample ranges from M0 to M5. The derived effective temperature and surface gravity range from 4000–3000 K and 4.5–5.5 dex, respectively. In most of the cases, the derived spectral types are in good agreement with previously assigned photometric classifications.

Key words: instrumentation: spectrograph, techniques: spectroscopy, stars: low-mass – M dwarfs – stellar atmosphere – fundamental parameters.

1 INTRODUCTION

Small-aperture (1–2 m class) telescopes, when equipped with suitable instrumentation, can broaden and diversify the scope of various science programmes that can be done with such facilities. The recent development of the Mt Abu Faint Object Spectrograph and Camera – Pathfinder (MFOSC-P) instrument (Srivastava et al. 2018) for the Physical Research Laboratory (PRL) 1.2 m optical–near-infrared (NIR) telescope at Mt Abu, India offers one such opportunity. The instrument has been developed to provide imaging and low-resolution spectroscopy ($R \sim 500$–2000) in the optical wavelength regime along the line of the widely used faint object spectrograph and camera (FOSC) series of instruments (e.g. EFOSC, Buzzoni et al. 1984; DFOSC, Andersen et al. 1995 etc.) and was commissioned on the telescope in 2019 February. Though MFOSC-P was conceived as a general user facility instrument for a variety of astrophysical science programmes, it can also be utilized for dedicated long-term observational programmes, e.g. understanding the exoplanet host-star properties. In coherence with the growing importance of exoplanet sciences, e.g. their environments, their host-star properties and their dependences, a dedicated exoplanet programme is being carried out using the purpose-built PARAS spectrograph with resolution $\sim$ 67 000 (Chakraborty et al. 2014, 2018a) on the 1.2 m PRL telescope. In coming years, the programme shall be further enhanced with the next-generation PARAS-2 spectrograph with a resolution $\sim$ 100 000 (Chakraborty et al. 2018b) on the upcoming 2.5 m PRL optical–NIR telescope at the same site. In general, M-dwarf candidates are of particular interest in planetary searches in the habitable zone as they offer suitable conditions in the solar neighbourhood with shorter orbital periods. Though their high-resolution spectroscopy is indeed useful for the detection and characterization of the host stars, their intrinsic low luminosities make them difficult targets for such high-resolution spectroscopy programmes on small-aperture telescopes. On the other hand, low-

★ E-mail: arvindr@prl.res.in (ASR); vipin@prl.res.in (VK); mudit@prl.res.in (MKS)

resolution spectrographs like MFOSC-P can target fainter objects and provide very useful insights regarding the host-star properties. Thus the feasibility of an M-dwarf characterization programme using low-resolution spectra from MFOSC-P was taken as a first dedicated science programme during the commissioning run of the instrument.

M dwarfs (0.6–0.075 $M_{\odot}$) are the most dominant stellar component and contribute around 40 per cent of the total stellar mass of the Galaxy (Chabrier 2003). In the recent past, various space-based as well as ground-based surveys (e.g. the *Wide-field Infrared Survey Explorer*, *WISE*, Wright et al. 2010; the Sloan Digital Sky Survey, SDSS, York et al. 2000; the Two Micron All Sky Survey, 2MASS, Skrutskie et al. 2006 etc.) have been extremely useful in providing unprecedented photometric and spectroscopic data of cool M dwarfs. Being suitable targets for various exoplanet search programmes, a good number of bright M-dwarf candidates in the solar neighbourhood have been surveyed for their photometry (Lépine & Gaidos 2011) and spectroscopy (Reid, Hawley & Gizis 1995; Hawley, Gizis & Reid 1996; Lépine et al. 2013; Frith et al. 2013). Survey such as the Palomar/Michigan State University (Palomar/MSU) Nearby-Star Spectroscopic Survey (Reid et al. 1995; Hawley et al. 1996) cover a sample of M dwarfs in both the Northern and Southern sky beyond the 25 pc limit with a radial velocity accuracy of $\pm$ 10 km s^{-1}. This survey was used to determine the spectral types, absolute magnitudes and distances of their targets, to identify chromospherically active M dwarfs with Hα emission and to determine the luminosity function (Reid et al. 1995; Hawley et al. 1996). The Palomar/MSU survey was further used by Hawley et al. (1996) and Gizis, Reid & Hawley (2002) to study the relation between chromospheric activity and age among early (M0–M2.5) and mid (M3–M6) dwarfs. Later, Lépine et al. (2013) and Frith et al. (2013) performed spectroscopic observations of bright M dwarfs (magnitude $J < 9$ and $K < 9$ respectively) in the Northern sky, as selected from the SUPERBLINK proper motion catalogue and Position and Proper Motion Extended-L (PPMXL) catalogue. Such surveys and programmes provide an insight into the age, metallicity and evolution of M dwarfs along with local star-formation history.

The determination of fundamental parameters (e.g. effective temperature, metallicity, surface gravity etc.) and atmospheric properties of M dwarfs from their spectra is also of great significance. However, the atmospheric properties of M dwarfs change significantly from early M dwarfs to late M dwarfs (M0–M9). The presence of complex molecular bands (e.g. titanium oxide, TiO, vanadium oxide, VO, in the optical and hydrides such as CaH, FeH in the NIR spectra of M dwarfs etc.) makes access to the M dwarfs' true continuum very difficult and causes uncertainties in the determination of their atmospheric properties and fundamental parameters. Recently, Rajpurohit et al. (2013, 2014, 2016, 2018a, 2018b), Passegger, Wende-von Berg & Reiners (2016) and Passegger et al. (2019) compared observed optical and NIR spectra of M dwarfs with their synthetic spectra to determine their atmospheric properties and fundamental parameters. Model atmospheres, such as BT-Settl, which accounts for recent advancements in various line lists by Plez (1998) and Barber et al. (2006), along with dust formation (Allard et al. 2003, 2012, 2013), are now able to reproduce the shape of the spectral energy distribution (SED) down to late M dwarfs (M9) and have improved the previous estimates significantly from earlier studies (Allard & Hauschildt 1995; Rajpurohit et al. 2012).

The principal aim of this paper is to perform spectroscopic observations to classify and determine the atmospheric properties and fundamental parameters of a sample of M dwarfs, thereby showing the importance of suitable instrumentation on small-aperture telescopes for M-dwarf studies and the usefulness of MFOSC-P for such programmes in particular. Our sample of M dwarfs along with the observations and data reduction are described in Section 2. Section 3 describes the spectroscopic classification based on the comparison with the template spectra. The determination of the fundamental parameters of the M dwarfs in our sample is described in Section 4. Section 5 discusses the Hα emission detected in M dwarfs. In Section 6 we discuss and summarize our results.

2 SPECTROSCOPIC OBSERVATIONS AND DATA REDUCTION

The observations were performed during the commissioning run of the MFOSC-P instrument on the PRL 1.2 m, f/13 telescope. We selected bright M-dwarf sources from the all-sky catalogue of bright M dwarfs (Lépine & Gaidos 2011), typically with V magnitude higher than 14 and covering a wide range of subspectral types. A total of 80 suitable targets were observed between 2019 February and June. The authors refer to Lépine & Gaidos (2011) for more details on the brightest M-dwarf candidates with magnitude $J < 10$. The details of these targets are summarized in Table 1. The parallaxes for these sources are obtained from the *Gaia* DR-2 archive (Luri et al. 2018) and are given as a reference. These parallaxes are converted to distance (pc) as per the method and tool given in Luri et al. (2018). All of these sources are within a distance of 100 pc.

MFOSC-P is a fully in-house-developed camera and spectrograph based on the concept of the faint object camera and spectrograph (FOSC) series of instruments. The instrument provides seeing-limited imaging with a sampling of 3.3 pixels per arcsec over a field of view of 5.2 × 5.2 square arcmin. MFOSC-P uses three plane reflection gratings with 500, 300 and 150 line-pairs (lp) mm^{-1} to provide slit-limited resolutions with dispersion of ∼1.1 Å per pixel, 1.9 Å per pixel and 3.8 Å per pixel respectively. Two slits of 75 and 100 μm width (corresponding to 1.0 and 1.3 arcsec on the sky) are provided for varying seeing conditions. For more details regarding the MFOSC-P instrument, the reader is referred to Srivastava et al. (2018). Another paper on the development, commissioning and characterization of the instrument is currently in preparation. The target M dwarfs in our sample were observed using 150 lp mm^{-1} grating covering a spectral range of 4800–8300 Å with a slit width of 1 arcsec. The sources were observed for integration times in the range of 500–1500 s per object. Wavelength calibration spectra were recorded immediately after each of the science spectra at the same instrument settings and telescope orientation. The MFOSC-P instrument is equipped with halogen and spectral calibration lamps. Neon and xenon calibration lamps are used for wavelength calibration. Spectrophotometric standard stars from the ESO catalogue [1] were also observed for the instrument response correction.

The raw data were later reduced using self-developed data-analysis routines in PYTHON using astronomical image processing libraries (e.g. ASTROPY etc.) available in the public domain. The steps include bias subtraction, cosmic ray removal, tracing and extracting the spectra, sky background subtraction etc. Pixel-to-pixel response variations were determined using halogen spectra; these were found to be less than 1 per cent and were thus not applied to the observed spectra. The wavelength solution was determined from the spectral-lamp spectra recorded

[1] https://www.eso.org/sci/observing/tools/standards/spectra/stanlis.html

Table 1. Properties of the M-dwarf sample used in this study along with their coordinates. Optical and near-infrared photometry is compiled from Ochsenbein, Bauer & Marcout (2000) and Lépine & Gaidos (2011). The parallaxes of the M dwarfs in our sample are taken from the *Gaia* DR-2 database (Luri et al. 2018).

Source Name	RA	Dec.	V (mag)	R (mag)	I (mag)	J (mag)	H (mag)	K (mag)	*Gaia* parallax (mas)	Distance (pc)
Css833	$13^h48^m34\overset{s}{.}02$	$+31°59'56\overset{''}{.}89$	12.34	11.91	–	9.02	8.43	8.22	34.083	29.34
G123-74	$12^h57^m32\overset{s}{.}41$	$+40°57'00\overset{''}{.}89$	13.23	12.43	10.20	9.22	8.57	8.38	24.400	40.98
G138-64	$16^h46^m13\overset{s}{.}76$	$+16°28'41\overset{''}{.}08$	11.65	10.60	9.27	7.95	7.29	7.09	63.407	15.77
G138-7	$16^h11^m28\overset{s}{.}10$	$+07°03'59\overset{''}{.}98$	14.08	13.41	10.60	9.77	9.28	9.02	36.411	27.46
G177-8	$12^h58^m17\overset{s}{.}17$	$+52°36'43\overset{''}{.}70$	13.19	12.40	10.40	9.29	8.72	8.50	38.105	26.24
G19-12	$17^h04^m49\overset{s}{.}57$	$+01°30'35\overset{''}{.}47$	13.47	12.92	10.90	9.60	8.97	8.75	–	–
GJ3584	$10^h04^m32\overset{s}{.}76$	$+05°33'41\overset{''}{.}25$	12.67	12.22	9.90	9.02	8.40	8.18	–	–
GJ3696	$11^h58^m17\overset{s}{.}61$	$+42°34'28\overset{''}{.}96$	14.43	13.76	10.60	9.59	8.98	8.71	46.028	21.73
GJ3697	$11^h58^m59\overset{s}{.}45$	$+42°39'39\overset{''}{.}81$	12.09	11.65	9.90	8.64	8.05	7.82	–	–
GJ3763	$13^h08^m50\overset{s}{.}52$	$+16°22'03\overset{''}{.}58$	13.48	12.71	10.20	9.26	8.65	8.41	35.918	27.84
GJ3793	$13^h34^m49\overset{s}{.}35$	$+20°11'38\overset{''}{.}67$	14.25	13.42	10.80	9.67	9.10	8.85	18.232	54.85
GJ3822	$14^h02^m19\overset{s}{.}62$	$+13°41'22\overset{''}{.}76$	10.64	9.69	8.68	7.56	6.89	6.71	49.175	20.34
GJ3873	$14^h54^m27\overset{s}{.}92$	$+35°32'56\overset{''}{.}94$	12.55	12.13	9.50	8.24	7.71	7.47	67.072	14.91
GJ3895	$15^h11^m55\overset{s}{.}96$	$+17°57'16\overset{''}{.}42$	13.98	12.90	10.60	9.56	9.06	8.77	41.228	24.26
LP324-18	$13^h51^m45\overset{s}{.}13$	$+31°42'57\overset{''}{.}67$	13.40	12.46	10.60	9.59	8.93	8.75	14.402	69.44
LP324-72	$14^h08^m10\overset{s}{.}47$	$+28°11'13\overset{''}{.}93$	12.75	12.31	10.60	9.73	9.06	8.90	19.749	50.64
LP378-897	$13^h16^m40\overset{s}{.}56$	$+23°15'42\overset{''}{.}43$	13.51	13.03	10.70	9.76	9.11	8.85	27.695	36.11
LP435-110	$12^h26^m38\overset{s}{.}10$	$+17°28'11\overset{''}{.}14$	13.63	12.74	10.50	9.64	9.01	8.79	25.938	38.55
LP671-33	$10^h46^m07\overset{s}{.}05$	$-08°22'14\overset{''}{.}77$	12.74	12.32	11.00	9.86	9.21	9.03	17.702	56.49
LP738-44	$13^h37^m30\overset{s}{.}00$	$-10°48'34\overset{''}{.}92$	12.46	12.10	–	9.73	9.09	8.91	–	–
StKM1-1125	$14^h08^m40\overset{s}{.}58$	$+23°50'54\overset{''}{.}94$	12.34	11.86	10.20	9.29	8.62	8.40	20.267	49.34
StKM1-1077	$13^h35^m16\overset{s}{.}12$	$+30°10'56\overset{''}{.}67$	11.67	11.30	–	8.76	8.14	7.91	25.689	38.93
StM186	$13^h41^m27\overset{s}{.}65$	$+48°54'45\overset{''}{.}87$	12.98	12.62	10.20	9.00	8.45	8.19	–	–
TYC2009-522-1	$14^h04^m10\overset{s}{.}24$	$+26°26'24\overset{''}{.}02$	12.33	11.92	–	9.83	9.21	9.03	14.545	68.75
UCAC3 160-122037	$13^h16^m49\overset{s}{.}39$	$-10°19'18\overset{''}{.}27$	13.92	13.71	11.29	9.97	9.43	9.11	–	10.00
UCAC4 396-055485	$13^h21^m56\overset{s}{.}31$	$-10°52'09\overset{''}{.}88$	13.90	13.70	11.00	9.52	8.82	8.62	18.818	53.14
UCAC4 407-056568	$13^h26^m56\overset{s}{.}92$	$-08°45'47\overset{''}{.}01$	12.99	12.58	–	9.45	8.86	8.59	–	–
UCAC4 407-057475	$13^h55^m12\overset{s}{.}70$	$-08°42'25\overset{''}{.}93$	13.00	12.80	–	9.25	8.65	8.40	28.976	34.51
UCAC4 421-056421	$12^h06^m07\overset{s}{.}44$	$-05°50'01\overset{''}{.}88$	13.16	12.77	–	9.97	9.33	9.06	18.425	54.27
UCAC4 436-076101	$18^h25^m48\overset{s}{.}64$	$-02°58'17\overset{''}{.}15$	13.05	12.64	–	9.62	8.95	8.75	21.076	47.45
UCAC4 448-055886	$13^h26^m26\overset{s}{.}40$	$-00°26'52\overset{''}{.}86$	12.48	12.07	–	9.89	9.28	9.08	13.105	76.31
UCAC4 450-057508	$15^h09^m50\overset{s}{.}64$	$-00°07'51\overset{''}{.}77$	12.33	11.91	–	9.51	8.90	8.69	19.318	51.77
UCAC4 451-054724	$13^h27^m06\overset{s}{.}68$	$+00°00'48\overset{''}{.}29$	13.02	12.57	–	9.74	9.13	8.91	23.360	42.81
UCAC4 451-055381	$13^h51^m13\overset{s}{.}78$	$+00°04'26\overset{''}{.}98$	13.06	12.82	–	9.90	9.25	9.04	18.456	54.18
UCAC4 451-081123	$18^h27^m41\overset{s}{.}08$	$+00°11'15\overset{''}{.}07$	12.92	12.65	–	9.48	8.89	8.60	–	–
UCAC4 467-056893	$16^h50^m11\overset{s}{.}00$	$+03°14'40\overset{''}{.}08$	14.03	13.30	–	9.72	9.19	8.92	–	–
UCAC4 484-057552	$15^h29^m48\overset{s}{.}62$	$+06°38'16\overset{''}{.}52$	12.69	12.23	–	9.99	9.34	9.16	10.529	94.97
UCAC4 496-060421	$13^h37^m17\overset{s}{.}62$	$+09°08'00\overset{''}{.}56$	12.86	12.48	–	9.34	8.77	8.50	27.347	36.57
UCAC4 528-054911	$12^h44^m24\overset{s}{.}96$	$+15°32'12\overset{''}{.}49$	13.86	13.45	–	9.99	9.40	9.16	23.280	42.96
UCAC4 534-051996	$11^h52^m20\overset{s}{.}53$	$+16°40'19\overset{''}{.}14$	13.54	13.16	–	9.73	9.17	8.92	34.955	28.61
UCAC4 540-054017	$13^h27^m30\overset{s}{.}59$	$+17°48'08\overset{''}{.}31$	12.66	12.27	–	9.83	9.18	9.01	15.333	65.22
UCAC4 546-052448	$12^h54^m10\overset{s}{.}86$	$+19°01'16\overset{''}{.}66$	13.50	13.27	–	9.59	8.94	8.69	31.123	32.13
UCAC4 548-070636	$18^h20^m35\overset{s}{.}82$	$+19°27'55\overset{''}{.}67$	12.81	12.21	10.30	9.57	8.88	8.70	17.700	56.50
UCAC4 550-052262	$13^h15^m49\overset{s}{.}21$	$+19°57'07\overset{''}{.}95$	13.58	13.15	–	9.87	9.25	8.99	28.602	34.96
UCAC4 570-051422	$14^h08^m40\overset{s}{.}58$	$+23°50'54\overset{''}{.}94$	12.34	11.86	10.20	9.29	8.62	8.40	20.267	49.34
UCAC4 570-051538	$14^h14^m35\overset{s}{.}09$	$+23°57'24\overset{''}{.}84$	12.53	12.39	10.70	9.78	9.13	8.98	13.737	72.80
UCAC4 574-047909	$12^h35^m33\overset{s}{.}43$	$+24°39'18\overset{''}{.}44$	13.43	13.05	10.80	9.93	9.25	9.06	13.174	75.91
UCAC4 587-051209	$15^h11^m04\overset{s}{.}82$	$+27°12'44\overset{''}{.}71$	13.13	12.58	10.60	9.53	8.93	8.70	24.985	40.02
UCAC4 599-049146	$11^h59^m13\overset{s}{.}54$	$+29°36'09\overset{''}{.}07$	13.26	12.64	–	9.89	9.34	9.11	–	–
UCAC4 605-050828	$14^h04^m08\overset{s}{.}56$	$+30°49'34\overset{''}{.}50$	13.03	12.54	–	9.43	8.76	8.52	26.001	38.46
UCAC4 607-049137	$14^h10^m15\overset{s}{.}46$	$+31°15'36\overset{''}{.}55$	13.86	13.26	–	9.96	9.30	9.03	–	–
UCAC4 615-064218	$18^h44^m20\overset{s}{.}37$	$+32°50'46\overset{''}{.}33$	13.73	13.06	–	9.65	9.05	8.80	29.039	34.44
UCAC4 629-047283	$13^h25^m55\overset{s}{.}16$	$+35°46'42\overset{''}{.}88$	13.48	12.82	10.40	9.64	9.09	8.84	29.349	34.07
UCAC4 630-046962	$11^h52^m57\overset{s}{.}15$	$+35°54'45\overset{''}{.}91$	13.69	13.41	11.20	9.96	9.35	9.13	25.112	39.82
UCAC4 640-048822	$14^h07^m07\overset{s}{.}51$	$+37°52'22\overset{''}{.}99$	12.57	12.17	10.50	9.67	9.02	8.83	17.232	58.03
UCAC4 641-058022	$18^h06^m17\overset{s}{.}74$	$+38°01'49\overset{''}{.}79$	12.23	11.55	10.20	9.32	8.66	8.48	8.670	115.34
UCAC4 647-050041	$12^h54^m29\overset{s}{.}25$	$+39°19'56\overset{''}{.}78$	13.32	12.89	10.70	9.97	9.35	9.13	19.221	52.03
UCAC4 687-054755	$13^h25^m18\overset{s}{.}24$	$+47°20'37\overset{''}{.}32$	12.68	12.16	10.50	9.74	9.12	8.89	17.925	55.79
UCAC4 719-054147	$15^h25^m48\overset{s}{.}82$	$+53°44'16\overset{''}{.}30$	12.70	12.26	–	9.86	9.21	9.02	17.079	58.55
UCAC4 724-051511	$13^h27^m01\overset{s}{.}69$	$+54°36'13\overset{''}{.}77$	12.88	12.61	10.90	9.87	9.27	9.04	19.643	50.91
UCAC4 731-051425	$13^h17^m23\overset{s}{.}17$	$+56°10'13\overset{''}{.}50$	13.38	13.09	10.80	9.80	9.22	8.98	26.768	37.36
UCAC4 780-025091	$13^h11^m59\overset{s}{.}55$	$+65°50'01\overset{''}{.}79$	12.95	12.58	10.60	9.71	9.06	8.84	27.740	36.05
UCAC4 413-059942	$14^h16^m33\overset{s}{.}28$	$-07°25'38\overset{''}{.}24$	13.76	13.47	–	9.81	9.20	8.94	17.242	58.00

Table 1 – *continued*

Source Name	RA	Dec.	*V* (mag)	*R* (mag)	*I* (mag)	*J* (mag)	*H* (mag)	*K* (mag)	*Gaia* parallax (mas)	Distance (pc)
UCAC4 413-060157	$14^h23^m01^s.24$	$-07°34'01''.11$	13.20	12.92	10.38	9.59	8.99	8.73	31.004	32.25
UCAC4 457-046840	$10^h06^m21^s.82$	$+01°21'23''.18$	13.77	13.57	–	9.53	9.00	8.70	39.547	25.29
UCAC4 462-046617	$10^h35^m46^s.92$	$+02°15'58''.21$	13.57	13.23	–	9.83	9.22	8.97	–	–
UCAC4 492-058611	$13^h49^m07^s.33$	$+08°23'36''.09$	12.18	11.67	–	9.34	8.76	8.55	17.878	55.94
UCAC4 518-059332	$15^h47^m11^s.96$	$+13°34'40''.78$	13.15	12.78	–	9.89	9.20	9.03	–	–
UCAC4 529-059437	$16^h27^m46^s.42$	$+15°42'06''.13$	13.16	12.70	11.10	9.98	9.38	9.17	20.594	48.56
UCAC4 536-067333	$17^h44^m12^s.95$	$+17°06'12''.14$	13.32	12.81	10.80	9.94	9.32	9.11	19.410	51.52
UCAC4 537-053981	$13^h35^m12^s.46$	$+17°14'08''.88$	13.19	12.73	10.80	9.87	9.21	9.03	13.898	71.95
UCAC4 544-056450	$15^h51^m39^s.13$	$+18°40'23''.54$	13.05	12.53	10.60	9.80	9.11	8.90	20.595	48.56
UCAC4 547-049435	$11^h05^m19^s.44$	$+19°18'34''.24$	13.82	13.35	–	9.87	9.28	9.01	23.696	42.20
UCAC4 562-051219	$12^h23^m43^s.46$	$+22°15'17''.08$	12.36	11.95	10.50	9.89	9.31	9.14	10.281	97.27
UCAC4 562-057449	$16^h38^m25^s.33$	$+22°22'41''.54$	13.06	12.54	10.80	9.61	9.05	8.82	30.562	32.72
UCAC4 598-053572	$15^h39^m05^s.72$	$+29°31'40''.62$	13.11	12.65	–	9.76	9.18	8.94	23.604	42.37
UCAC4 629-050950	$16^h27^m37^s.57$	$+35°41'42''.94$	13.71	13.31	10.60	9.60	9.02	8.74	35.924	27.84
UCAC4 647-048900	$11^h31^m16^s.41$	$+39°23'02''.91$	13.05	12.64	10.60	9.70	9.12	8.88	27.390	36.51
UCAC4 682-053954	$14^h13^m46^s.76$	$+46°18'22''.73$	13.14	12.64	10.40	9.43	8.80	8.59	25.434	39.32
UCAC4 507-054072	$13^h15^m47^s.39$	$+11°16'25''.77$	13.20	12.77	–	9.76	9.16	8.95	19.186	52.12

immediately after the science observations. A third-order polynomial fit was used to generate the pixel versus wavelength relation.

Though second-order contamination from the blue part is expected to be present in the redder part of the spectrum, targets like M dwarfs are redder in spectrum and typically have *U*- to *I*-band flux ratios of nearly 1:100. Thus, given the spectral throughput of the instrument along with the telescope in the blue part, the blaze function of the grating and the spectral energy distribution (SED) of the objects, second-order spectral contamination is minimal. Nevertheless, even though the observed spectral range is up to 8300 Å, we have restricted our analysis to a wavelength range of 4800–8100 Å (see Sections 3 and 4).

3 FOLLOW-UP SPECTROSCOPIC CLASSIFICATION

Over the last few decades, several schemes have been proposed for M-dwarf classification. These schemes, mostly based on the spectral shape and features of the M-dwarf spectra, are used to preliminarily classify them according to their fundamental parameters and atmospheric properties.

The spectral energy distribution (SED) and the broadband colours of M dwarfs are mostly governed by the various molecular opacities, e.g. TiO, VO and hydrides bands etc., both in the optical and in the NIR. The strengths of these opacities vary from early-type M dwarf (M0 type) to late-type (M5 or later); for example, broad molecular bands such as those from TiO are stronger in early M dwarfs while the VO and hydride (CaH) bands are stronger (Allard, Hauschildt & Schwenke 2000) in later M dwarfs. The strength of these molecular bands depends on the atmospheric properties and various stellar parameters such as the effective temperature ($T_{\rm eff}$), surface gravity ($\log g$) and metallicity ([M/H]) of the M dwarf. Considering such variation in the M-dwarf spectra, Kirkpatrick, Henry & McCarthy (1991) used the least-squares minimization technique to classify M dwarfs by comparing the template M-dwarf spectra with the target spectrum. Later on Henry et al. (2002) and Scholz, Meusinger & Jahreiß (2005) used a similar technique that compares the low-resolution template spectra of M dwarfs with that of the observed M-dwarf spectrum.

Reid et al. (1995) adopted a classification scheme that was based on measurement of the strength of the most prominent molecular bands, called 'band indices', such as TiO and CaH. Here the ratio of the flux between various bandheads to that of the flux in the nearby pseudo-continuum was determined; this was then used to classify early M dwarfs to mid M dwarfs (M0–M5). These bands get saturated in late M dwarfs (later than M5); thus VO bandheads were used for the classification (Kirkpatrick, Henry & Simons 1995). Martín et al. (1999) assigned the spectral type to late M dwarfs based on the pseudo-continuum spectral ratios (namely PC3). Gizis (1997) further classified them into the subcategory of M subdwarfs based on the strength and ratio of the CaH and TiO molecular bandheads. This work was later expanded by Lépine, Shara & Rich (2003) and Lépine, Rich & Shara (2007).

While the above works utilize high-resolution spectra, Scholz et al. (2005) showed that a comparison of low-resolution spectral template provides an accurate classification of M dwarfs. In this work we have utilized the low-resolution spectra of M dwarfs covering the spectral regime 4800–8100 Å for their classification. The template spectra of low-mass M dwarfs are taken from Bochanski et al. (2007) to be used as template spectra of such stars from M0–L0. These template spectra were derived from 4000 SDSS spectra. Similar to the works of Kirkpatrick et al. (1995), Scholz et al. (2005), we have adopted least-squares minimization techniques to determine the spectral type of the observed M dwarfs in our sample.

Here we first normalized both the template and observed spectra of M dwarfs. The higher-resolution ($R \sim 1800$) SDSS template spectra were then convolved using a Gaussian kernel at the same resolution as that of the observed spectrum ($R \sim 500$). Later these flux-normalized spectra were compared with the template ones for the least-squares minimization process to obtain the nearest match. The spectral type of this nearest match was then assigned to the observed M dwarf (Table 2). We expect the error to be of one spectral class in this method as the template spectra themselves are at the spacing of one spectral class.

Fig. 1 shows the comparison of a set of observed spectral sequences of M dwarfs in our sample with the SDSS standard M-dwarf template spectra along with the most prominent spectral features. We also tried to classify the M dwarfs in our sample by using the spectral-index method developed by Reid et al. (1995)

Table 2. Stellar parameters of the M-dwarf sample determined in this study.

Source Name	Photometric Spectral type (Lépine & Gaidos 2011)	Derived Spectral type (This study)	$T_{\rm eff}$ (K)	log g (cm s^{-2})	Source Name	Photometric Spectral type (Lépine & Gaidos 2011)	Derived Spectral type (This study)	$T_{\rm eff}$ (K)	log g (cm s^{-2})
Css833	M2	M2	3500	5	UCAC4 540-054017	M0	M1	3700	5
G123-74	M3	M2	3500	5.5	UCAC4 546-052448	M4	M4	3200	4.5
G138-64	M3	M4	3200	5	UCAC4 548-070636	M2	M2	3500	5
G138-7	M4	M4	3200	5	UCAC4 550-052262	M3	M3	3400	4.5
G177-8	M3	M4	3200	5	UCAC4 570-051422	M1	M1	3700	5.5
G19-12	M3	M4	3300	5	UCAC4 570-051538	M1	M1	3600	5
GJ3584	M3	M3	3400	4.5	UCAC4 574-047909*	M3	M3	3400	5
GJ3696	M5	M5	3100	5.5	UCAC4 587-051209	M2	M2	3400	5
GJ3697	M2	M2	3500	4.5	UCAC4 599-049146	M2	M2	3500	5
GJ3763	M4	M3	3400	4.5	UCAC4 605-050828	M3	M3	3400	5
GJ3793	M4	M4	3200	5	UCAC4 607-049137	M3	M3	3400	5
GJ3822	M0	M1	3700	5.5	UCAC4 615-064218	M3	M3	3300	5
GJ3873	M4	M4	3200	5	UCAC4 629-047283	M3	M3	3400	5
GJ3895	M4	M3	3300	4.5	UCAC4 630-046962*	M3	M3	3300	5
LP324-18	M3	M1	3600	5.5	UCAC4 640-048822	M1	M1	3700	5
LP324-72	M0	M2	3600	5	UCAC4 641-058022	M0	M1	3700	5
LP378-897	M4	M3	3300	5	UCAC4 647-050041	M2	M3	3400	5
LP435-110	M3	M3	3400	4.5	UCAC4 687-054755	M1	M1	3600	5
LP671-33	M0	M1	3700	5.5	UCAC4 719-054147	M1	M1	3600	5
LP738-44	M0	M0	3800	5.5	UCAC4 724-051511	M2	M2	3500	5
StKM1-1125	M1	M2	3600	5	UCAC4 731-051425	M4	M3	3300	5
StKM1-1077	M0	M1	3800	5.5	UCAC4 780-025091	M2	M3	3300	5
StM186	M4	M3	3400	4.5	UCAC4 413-059942*	M4	M4	3300	5
TYC2009-522-1	M0	M0	3900	5	UCAC4 413-060157	M1	M3	3400	4.5
UCAC3 160-122037*	M4	M4	3200	5	UCAC4 457-046840	M4	M5	3100	5
UCAC4 396-055485*	M4	M5	3000	5	UCAC4 462-046617*	M3	M4	3300	5
UCAC4 407-056568	M3	M3	3400	4.5	UCAC4 492-058611	M0	M1	3700	5
UCAC4 407-057475	M3	M3	3400	4.5	UCAC4 518-059332	M3	M2	3500	5
UCAC4 421-056421	M3	M2	3600	5	UCAC4 529-059437	M3	M2	3600	5
UCAC4 436-076101	M2	M3	3400	5	UCAC4 536-067333	M3	M3	3500	4.5
UCAC4 448-055886	M1	M0	3800	5.5	UCAC4 537-053981*	M3	M2	3600	5
UCAC4 450-057508	M0	M1	3700	5	UCAC4 544-056450*	M2	M2	3600	5
UCAC4 451-054724	M2	M2	3500	5	UCAC4 547-049435	M4	M4	3200	5
UCAC4 451-055381	M2	M1	3600	5	UCAC4 562-051219	M0	M0	3900	5
UCAC4 451-081123	M3	M4	3300	5	UCAC4 562-057449	M3	M3	3500	4.5
UCAC4 467-056893	M4	M3	3300	5	UCAC4 598-053572	M3	M2	3400	5
UCAC4 484-057552	M1	M1	3800	5.5	UCAC4 629-050950*	M4	M4	3200	5
UCAC4 496-060421	M0	M3	3400	5	UCAC4 647-048900	M2	M3	3400	5
UCAC4 528-054911	M4	M4	3200	5	UCAC4 682-053954*	M3	M3	3300	5
UCAC4 534-051996	M4	M3	3300	5	UCAC4 507-054072	M3	M3	3400	4.5

Note. *Hα emission at 6563 Å is detected.

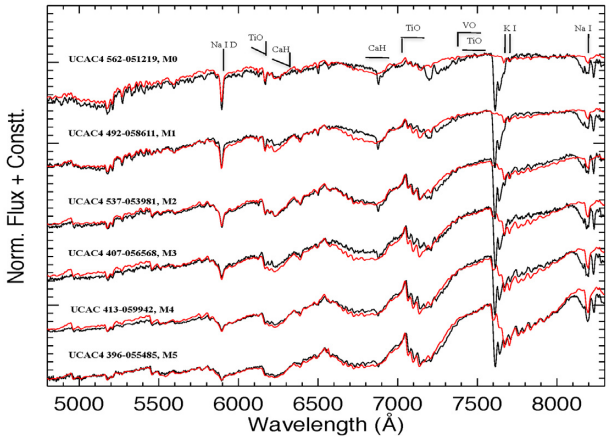

Figure 1. SDSS template spectra (red) taken from Bochanski et al. (2007) are compared with the observed spectral sequence of M dwarfs (black). Representative spectra of different subclasses from our sample are chosen to show the match. The most prominent spectral features along with the derived spectral type are also labelled.

using the band strengths of TiO and CaH. However, the resolution of our spectra was not good enough to achieve reliable spectral types. Figs 2, 3 and 4 show the observed spectra of M dwarfs in our sample along with their spectral type derived from the method describe above. Most of the sources shows similar spectral subclassifications or are within one class of their photometric classification (Lépine & Gaidos 2011). In four cases the difference is two or three subclasses.

4 FUNDAMENTAL PARAMETERS

The fundamental stellar parameters of our sample targets were determined by comparing the observed spectra with the synthetic spectra generated by the BT-Settl version of PHOENIX (Allard, Homeier & Freytag 2010, ; Allard et al. 2013). The BT-Settl model grid spans a $T_{\rm eff}$ range between 300 and 7000 K in steps of 100 K, log g ranges from 2.5–5.5 dex in steps of 0.5 dex and metallicity [M/H] ranges from −2.5 to +0.5 dex in steps of 0.5 dex. These models account for the latest solar abundances by Caffau et al. (2009), Caffau et al. (2011) with updated water vapour opacities (Barber & Tennyson 2008). Various microphysical processes as

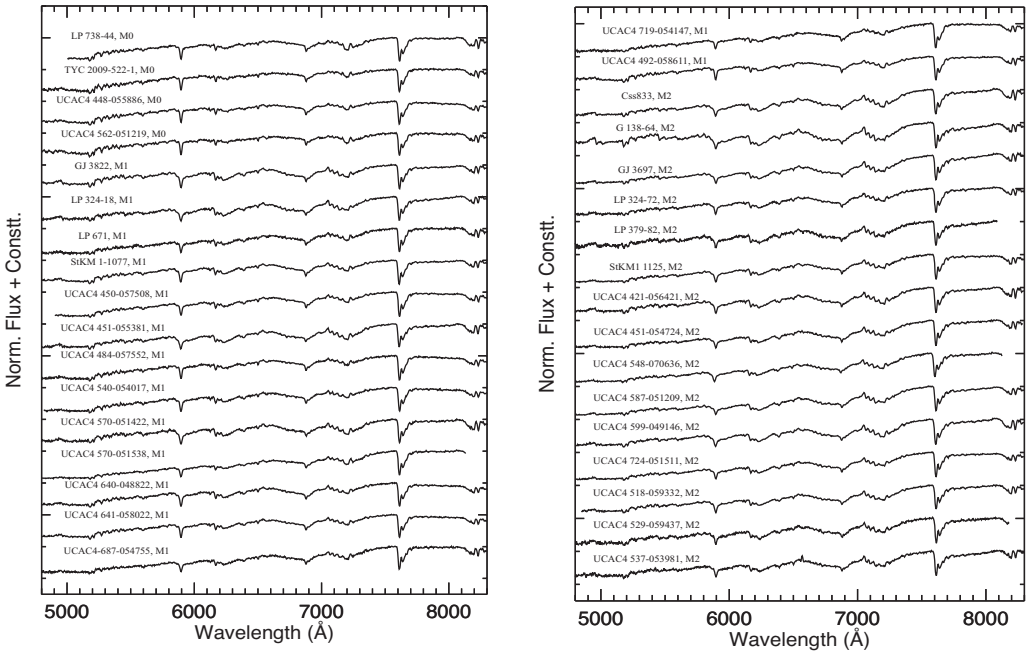

Figure 2. Optical spectra of M dwarfs from the spectral sequence M0–M2 observed with the MFOSC.

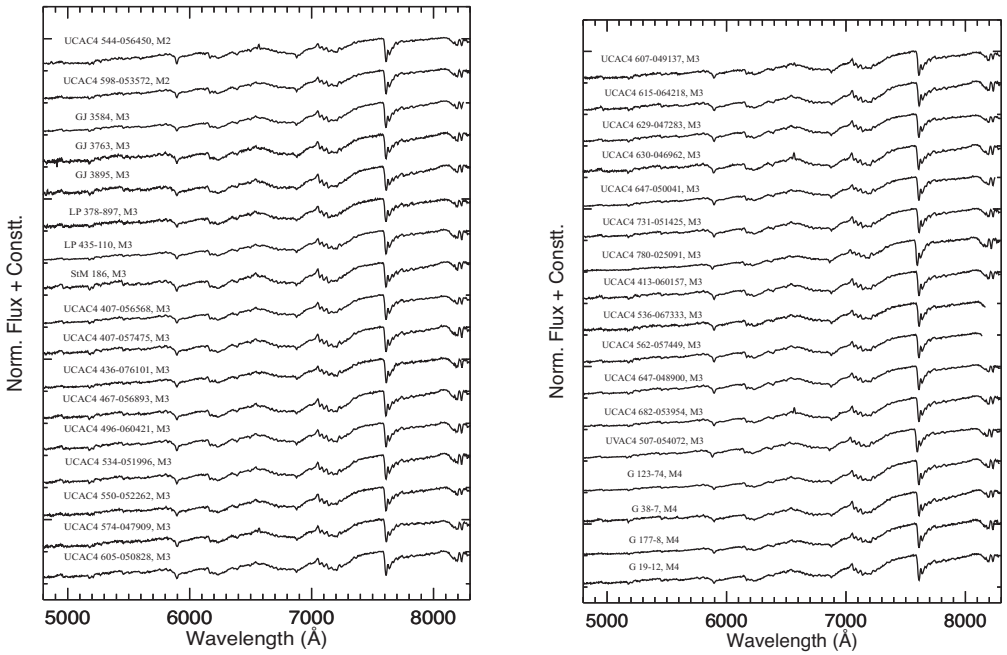

Figure 3. Same as Fig. 2 but for the spectral sequence from M2–M4.

well as dust and cloud formation along with the gravitational settling (Allard et al. 2012) have also been included in these models. Recently, Rajpurohit et al. (2012, 2013, 2014, 2018a, 2018b) have validated the BT-Settl models by comparing the low-resolution ($\triangle\lambda$ = 10 Å) as well as the high-resolution (R = 20 000 and 90 000) optical and NIR with the BT-Settl models in the grid range of $2400 \leq T_{\rm eff} \leq 4000$ K.

The BT-Settl model grid used in this study for the comparison spans $T_{\rm eff}$ between 3000 and 4000 K in steps of 100 K and log g ranges from 4.0–5.5 dex in steps of 0.5 dex. Since the M dwarfs in our sample lie within 100 pc of the solar neighbourhood and belong to the disc population (Lépine & Gaidos 2011), we do not expect large deviations from solar metallicity. Thus we used models with solar metallicity ([M/H] = 0.0) for comparison. The comparison of BT-Settl synthetic spectra with the observed spectra involves the process of degrading the high-resolution synthetic spectra at a resolution of the observed spectra by using a Gaussian convolution. We then employed the χ^2 method as discussed in Rajpurohit et al. (2013) to determine the $T_{\rm eff}$ and log g of M dwarfs in our sample. A spectral range between 5500 and 8100 Å was used for the χ^2 calculation. The spectral regions below 5500 Å (due to low SNR) and between 7600 and 7700 Å (which includes telluric

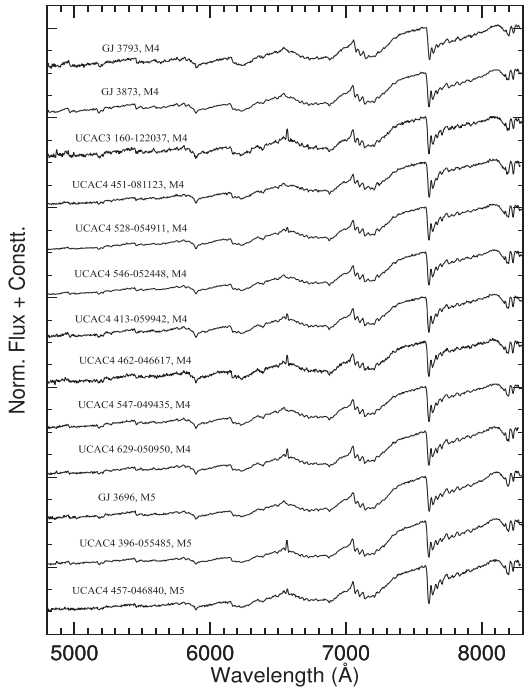

Figure 4. Same as Fig. 2 but for the spectral sequence from M4–M5.

absorption) were not considered in the χ^2 calculations. During the χ^2 calculations, we did not apply any weights on any spectral region for the determination of $T_{\rm eff}$ and log g. We retained the models that give the lowest χ^2 as the best-fitting parameters. The best-fitting models were also inspected visually by comparing them with the observed spectra. With the given resolution of the observed spectra the error in the derived fundamental parameters is equal to the grid spacing of the synthetic spectrum, which is 100 K for $T_{\rm eff}$ and 0.5 dex for log g. More details about the procedure for the determination of the stellar parameters of M dwarfs can be found in Rajpurohit et al. (2013). The BT-Settl model is able to reproduce the shape of SED and the profiles of strong atomic lines such as Na ID, though no attempt has been made to fit individual atomic lines, such as the K I and Na I resonance doublets. Figs 5, 6 and 7 show a comparison of the entire spectral sequence of M dwarfs (black) with the synthetic spectra (red). The best-fitting parameters of M dwarfs in our sample are given in Table 2. We have compared $T_{\rm eff}$ and spectral type determined for the individual stars in this study with Rajpurohit et al. (2013) and found a very good agreement between them (Fig. 8).

5 CHROMOSPHERIC ACTIVITY

With a thick convection zone above a radiative interior, the low-mass stars in particular M dwarfs show a high level of photospheric, chromospheric, and coronal magnetic activities. In this context, Hα emission at 6563 Å is of particular importance as this is an indicator of the chromospheric activity in the spectra of M dwarfs (Hawley et al. 1996; Gizis et al. 2002; Reiners & Basri 2008). Hawley et al. (1996) found that late-type M dwarfs, i.e. later than $>$ M5, show that the incidence of activity increases monotonically as compared to early M dwarfs. They also showed that the TiO band structure depends on the chromospheric activity level of the star and thus is very useful to constrain the atmospheric model of M dwarfs. Detailed studies of such activities in field M dwarfs and M dwarfs in open clusters is of great importance as they can be used to calibrate their age–activity relationship, to determine local star-formation history and to understand the substellar mass function (Gizis et al. 2002).

In our sample of 80 M dwarfs, we have detected Hα in 10 of them, which are listed in Table 2. We will be performing a follow-up

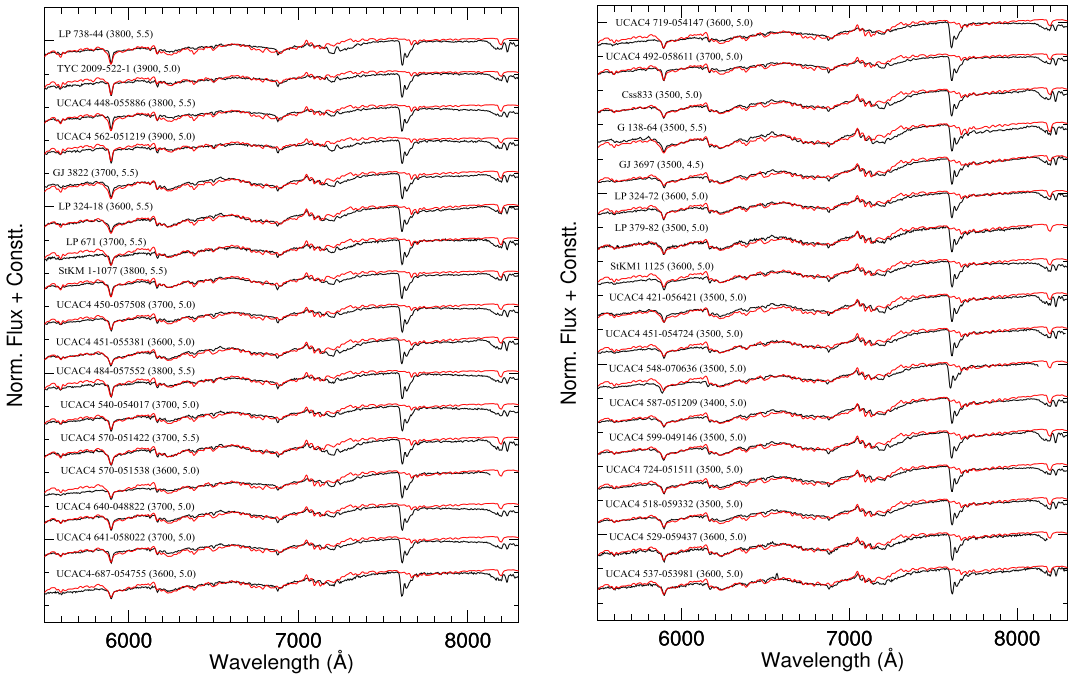

Figure 5. Comparison of observed spectra of M dwarfs (black) ranging from M0–M2, with the best-fitting BT-Settl synthetic spectra (red). The model displayed here has log g ranging from 4.5–5.5 dex and $T_{\rm eff}$ ranging from 3800–3400 K. Telluric features near 7600–7700 Å were ignored in the χ^2 calculation.

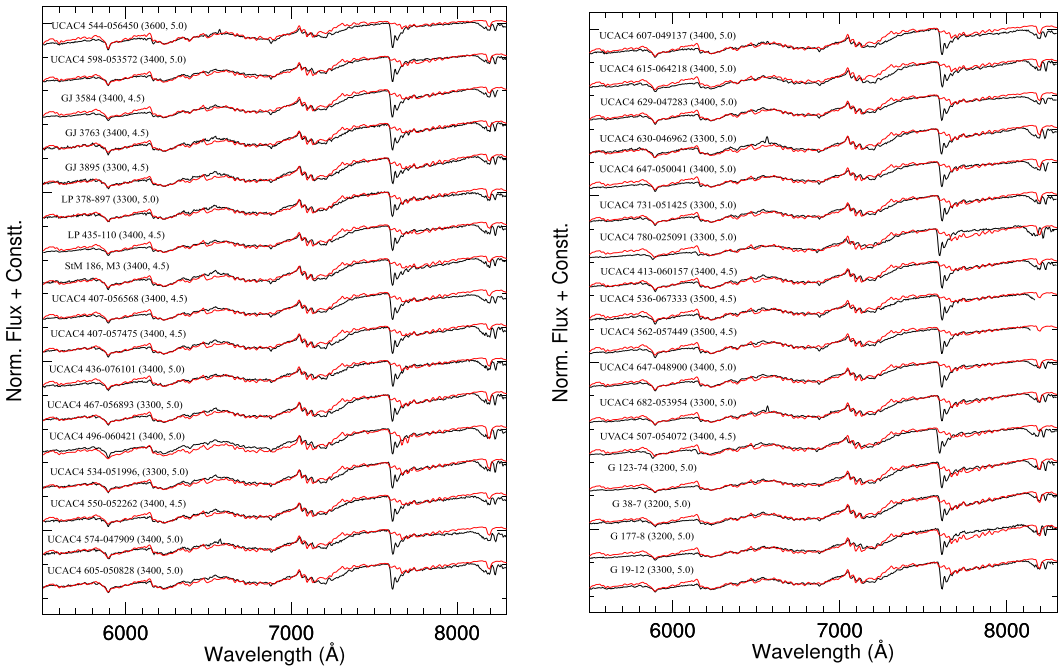

Figure 6. Same as Fig. 5 but for spectral type ranging from M2–M4. The model displayed here has log g ranging from 4.5–5.5 dex and $T_{\rm eff}$ ranging from 3600–3300 K.

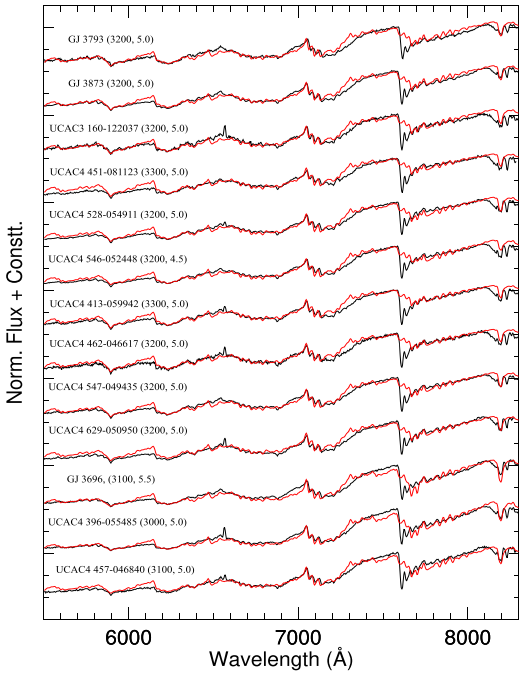

Figure 7. Same as Fig. 5 but for spectral type ranging from M4–M5. The model displayed here has log g ranging from 4.5–5.5 dex and $T_{\rm eff}$ ranging from 3300–3000 K.

spectroscopic study of the variability of the H α of these objects as well as other active M dwarfs in the literature, as a proxy for the magnetic variability using MFOSC-P. Such a follow-up study of these objects allow us to understand and correlate various properties such as age or rotation velocity as suggested by Hawley et al. (1996) and Gizis et al. (2002).

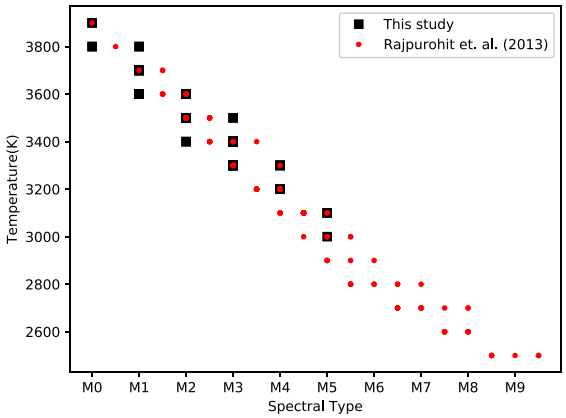

Figure 8. Comparison of the relationship between $T_{\rm eff}$ and spectral type from this study (solid black squares) with that of Rajpurohit et al. (2013) (solid red circles).

6 CONCLUSION

We have performed low-resolution spectroscopic follow-up observations of 80 bright M dwarfs. All the 80 M dwarfs used in this study have $J < 10$ magnitude and are identified from the all-sky catalogue of M dwarfs (Lépine & Gaidos 2011). We have spectroscopically classified all the M dwarfs in our sample by comparing them with the standard SDDS template spectra of M dwarfs and assigned spectral types to them. The spectral types of M dwarfs in our sample range from M0−M5.

We have used the most recent BT-Settl synthetic spectra (Allard et al. 2013) to perform a spectral synthesis analysis and determined the atmospheric parameters, in particular $T_{\rm eff}$ and log g within an uncertainty of 100 K in $T_{\rm eff}$ and 0.5 dex in log g. Our $T_{\rm eff}$ of M dwarfs ranges from 4000–3000 K and log g ranges from 4.5–5.5 dex and

is extended down to M dwarfs with spectral type M5. The recent BT-Settl model, which accounts for the revised solar abundances and TiO line list, is able to reproduce the SED of the M dwarfs of the entire spectral sequence.

The search for habitable planets around M dwarfs is one of the most exciting observation programmes of recent times. Though in the past such programmes were limited by the smaller number of high-resolution spectroscopy facilities and the faint nature of such objects, various dedicated upcoming facilities (e.g. high-precision radial velocity spectrographs on larger telescopes) are expected to give a big boost to these observation programmes. Such methods of high-resolution spectroscopy would not only help in the detection of newer planets but also in the studies of planets and host-star environments. While the role of high-resolution spectra is of great significance, a good deal of information about these objects can still be derived using low-resolution spectra on small-aperture telescopes. In this work we have attempted one such study for M dwarfs. The spectroscopic catalogue presented here, along with the spectral types and stellar parameters, is expected to provide a useful list of targets for such surveys. Detection of Hα emission in some of the targets here presents a case to study active M dwarfs with their short-term Hα variability and to understand rotation–activity relations in M dwarfs. Such programmes shall be explored in the future using the medium-resolution spectroscopy mode ($\delta\lambda \sim 2000$) of MFOSC-P.

ACKNOWLEDGEMENTS

The MFOSC-P instrument is funded by the Department of Space, Government of India through the Physical Research Laboratory. MKS thanks the Director, PRL for supporting the MFOSC-P development programme. The research leading to these results has received funding from the French 'Programme National de Physique Stellaire' and the Programme National de Planetologie of CNRS (INSU). The computations were performed at the Pôle Scientifique de Modélisation Numérique (PSMN) at the École Normale Supérieure (ENS) in Lyon, and at the Gesellschaft für Wissenschaftliche Datenverarbeitung Göttingen in collaboration with the Institut für Astrophysik Göttingen. DH was supported by the Collaborative Research Centre SFB 881 'The Milky Way System' (subproject A4) of the German Research Foundation (DFG). This work has made use of data from the European Space Agency (ESA) mission *Gaia* (https://www.cosmos.esa.int/gaia), processed by the *Gaia* Data Processing and Analysis Consortium (DPAC, https://www.cosmos.esa.int/web/gaia/dpac/consortium). Funding for the DPAC has been provided by national institutions, in particular the institutions participating in the *Gaia* Multilateral Agreement. This research has made use of the VizieR catalogue access tool, CDS, Strasbourg, France (DOI: 10.26093/cds/vizier). The authors thank the anonymous referee for his/her useful suggestions to improve the manuscript.

REFERENCES

Allard F., Hauschildt P. H., 1995, ApJ, 445, 433
Allard F., Hauschildt P. H., Schwenke D., 2000, ApJ, 540, 1005
Allard F., Guillot T., Ludwig H.-G., Hauschildt P. H., Schweitzer A., Alexander D. R., Ferguson J. W., 2003, in Martín E., ed., Proc. IAU Symp., Brown Dwarfs, Vol. 211, Astronomical Soceity of the Pacific, San Fransisco, p. 325
Allard F., Homeier D., Freytag B., 2010, in Christopher M. J-K, Matthew K. B., Andrew A. W., eds, Stellat Systems and the Sun, ASP Conference Series, Vol. 448, Proceedings of a Conference, Astronomical Soceity of the Pacific, San Fransisco, p. 91
Allard F., Homeier D., Freytag B., Sharp C. M., 2012, in Reylé C., Charbonnel C., Schultheis M., eds, EAS Publ. Ser., Vol. 57, Low Mass Stars and The Transition Stars/Brown Dwarfs-EES2011, p. 3
Allard F., Homeier D., Freytag B., Schaffenberger W., Rajpurohit A. S., 2013, Mem. Soc. Astron. Ital. Suppl., 24, 128
Andersen J. et al., 1995, Messenger, 79, 12
Barber R. J., Tennyson J., 2008, in European Planetary Science Congress 2008, Proceedings of the conference held 21-25 September 2008, Munster Germany, p. 870
Barber R. J., Tennyson J., Harris G. J., Tolchenov R. N., 2006, MNRAS, 368, 1087
Bochanski J. J., West A. A., Hawley S. L., Covey K. R., 2007, AJ, 133, 531
Buzzoni B. et al., 1984, Messenger, 38, 9
Caffau E., Maiorca E., Bonifacio P., Faraggiana R., Steffen M., Ludwig H.-G., Kamp I., Busso M., 2009, A&A, 498, 877
Caffau E., Ludwig H.-G., Steffen M., Freytag B., Bonifacio P., 2011, Sol. Phys., 268, 255
Chabrier G., 2003, ApJ, 586, L133
Chakraborty A. et al., 2014, PASP, 126, 133
Chakraborty A., Roy A., Sharma R., Mahadevan S., Chaturvedi P., Prasad N. J. S. S. V., Anandarao B. G., 2018a, AJ, 156, 3
Chakraborty A., Thapa N., Kumar K., Neelam P. J. S. S. V., Sharma R., Roy A., 2018b, in Proc. SPIE, Vol. 10702, Ground-based and Airborne Instrumentation for Astronomy VII: 107026G, SPIE Astronomical Telescope and Instrumentation, Austin Texas, USA, p. 107026G
Frith J. et al., 2013, MNRAS, 435, 2161
Gizis J. E., 1997, AJ, 113, 806
Gizis J. E., Reid I. N., Hawley S. L., 2002, AJ, 123, 3356
Hawley S. L., Gizis J. E., Reid I. N., 1996, AJ, 112, 2799
Henry T. J., Walkowicz L. M., Barto T. C., Golimowski D. A., 2002, AJ, 123, 2002
Kirkpatrick J. D., Henry T. J., McCarthy D. W. Jr, 1991, ApJS, 77, 417
Kirkpatrick J. D., Henry T. J., Simons D. A., 1995, AJ, 109, 797
Lépine S., Gaidos E., 2011, AJ, 142, 138
Lépine S., Shara M. M., Rich R. M., 2003, AJ, 126, 921
Lépine S., Rich R. M., Shara M. M., 2007, ApJ, 669, 1235
Lépine S., Hilton E. J., Mann A. W., Wilde M., Rojas-Ayala B., Cruz K. L., Gaidos E., 2013, AJ, 145, 102
Luri X. et al., 2018, A&A, 616, A9
Martín E. L., Delfosse X., Basri G., Goldman B., Forveille T., Zapatero Osorio M. R., 1999, AJ, 118, 2466
Ochsenbein F., Bauer P., Marcout J., 2000, A&AS, 143, 23
Passegger V. M., Wende-von Berg S., Reiners A., 2016, A&A, 587, A19
Passegger V. M. et al., 2019, Astronomy and Astrophysics, 627, 15
Plez B., 1998, A&A, 337, 495
Rajpurohit A. S. et al., 2012, A&A, 545, A85
Rajpurohit A. S., Reylé C., Allard F., Homeier D., Schultheis M., Bessell M. S., Robin A. C., 2013, A&A, 556, A15
Rajpurohit A. S., Reylé C., Allard F., Scholz R.-D., Homeier D., Schultheis M., Bayo A., 2014, A&A, 564, A90
Rajpurohit A. S., Reylé C., Allard F., Homeier D., Bayo A., Mousis O., Rajpurohit S., Fernández-Trincado J. G., 2016, A&A, 596, A33
Rajpurohit A. S., Allard F., Teixeira G. D. C., Homeier D., Rajpurohit S., Mousis O., 2018a, A&A, 610, A19
Rajpurohit A. S., Allard F., Rajpurohit S., Sharma R., Teixeira G. D. C., Mousis O., Kamlesh R., 2018b, A&A, 620, A180
Reid I. N., Hawley S. L., Gizis J. E., 1995, AJ, 110, 1838
Reiners A., Basri G., 2008, ApJ, 684, 1390
Scholz R. D., Meusinger H., Jahreiß H., 2005, A&A, 442, 211
Skrutskie M. F. et al., 2006, AJ, 131, 1163
Srivastava M. K., Jangra M., Dixit V., Munjal B. S., Arora H., Mavani T., 2018, in Proc. SPIE, Vol. 10702, Ground-based and Airborne Instrumentation for Astronomy VII: 107024I, SPIE Astronomical Telescope and Instrumentation, Austin Texas, USA, p. 107024I
Wright E. L. et al., 2010, AJ, 140, 1868
York D. G. et al., 2000, AJ, 120, 1579

This paper has been typeset from a TEX/LATEX file prepared by the author.